

Controlling the stability of both the structure and velocity of domain walls in magnetic nanowires

J. Brandão, and D. Atkinson

Citation: *Appl. Phys. Lett.* **109**, 062405 (2016);

View online: <https://doi.org/10.1063/1.4960201>

View Table of Contents: <http://aip.scitation.org/toc/apl/109/6>

Published by the [American Institute of Physics](#)

Articles you may be interested in

[The design and verification of MuMax3](#)

AIP Advances **4**, 107133 (2014); 10.1063/1.4899186

[Control of the magnetic vortex chirality in Permalloy nanowires with asymmetric notches](#)

Journal of Applied Physics **116**, 193902 (2014); 10.1063/1.4902008

[Trajectory and chirality of vortex domain walls in ferromagnetic nanowires with an asymmetric Y-branch](#)

Journal of Applied Physics **121**, 093905 (2017); 10.1063/1.4976967

[The effect of geometrical confinement and chirality on domain wall pinning behavior in planar nanowires](#)

Journal of Applied Physics **104**, 033904 (2008); 10.1063/1.2961313

[Controlling domain wall pinning in planar nanowires by selecting domain wall type and its application in a memory concept](#)

Applied Physics Letters **92**, 022510 (2008); 10.1063/1.2832771

[Stochastic domain wall depinning in permalloy nanowires with various types of notches](#)

AIP Advances **6**, 125124 (2016); 10.1063/1.4973647

Scilight

Sharp, quick summaries **illuminating**
the latest physics research

Sign up for **FREE!**



Controlling the stability of both the structure and velocity of domain walls in magnetic nanowires

J. Brandão and D. Atkinson

Centre for Materials Physics, Durham University, South Road, Durham DH1 3LE, United Kingdom

(Received 23 May 2016; accepted 21 July 2016; published online 10 August 2016)

For magnetic nanowire devices, the precise control of both domain wall (DW) motion and pinning behaviour is essential for reliable functional performance. The domain wall velocity and wall structure are typically sensitive to the driving field or spin-polarized current, and the pinning behaviour depends on the walls' structure and chirality, leading to variability in behaviour. Here, a systematic study combining experimental measurements and micromagnetic simulations of planar nanowires with small fixed-angle structural modulations on both edges was undertaken to study the domain wall reversal regime. A phase diagram for the reversal field as a function of modulation amplitude was obtained that shows that three DW reversal regime. A range of field and modulation amplitudes were identified in which stable DW reversal occurs, where the wall velocity is constant as a function of field and the wall structure is stable, which is well suited to applications.

Published by AIP Publishing. [<http://dx.doi.org/10.1063/1.4960201>]

Device concepts based on the movement and pinning of magnetic domain walls (DWs) in planar nanowires have been developing for more than a decade.^{1–9} Significant conceptual developments for non-volatile magnetic data storage^{11–13} and logic applications^{3–5} with in-plane magnetization have stimulated a lot of research. In the case of non-volatile data storage, research has moved on to device concepts in magnetic systems with out-of-plane magnetization, where the motion of interface modified domain walls^{14–16} and skyrmions^{17,18} form the basis of data storage and manipulation. Notwithstanding this, applications and device concepts for in-plane magnetized nanowires continue to develop for logic and sensing,^{10,19,20} and a wide range of concepts for biotechnology and medicine applications, including magnetic tagging, detection of proteins and cells, as well as sorting and drug delivery.^{21–23} These applications are driven to understanding and control DW behavior in nanowires with in-plane magnetization. For robust functional performance, DW behaviour needs to be highly repeatable in terms of both propagation and pinning; thus, variability in pinning behaviour or sensitivity of the propagation velocity to magnetic field will affect device reliability.

DW mechanisms such as nucleation, injection, and positional pinning have been explored as a route to improve the DW behavior.^{12,24–26} In simple nanostructures, domain wall motion is highly complex as a function of magnetic field amplitude which shows double (DVW) or triple (TVW) vortex walls.²⁷ Oscillations and stochasticity of the DW internal structure and precessional behavior limit reliability, leading to dynamic transitions and hence instability.^{28–30} For transverse domain walls (T-DWs), such oscillations are linked with a transformation to vortex (V-DWs)/anti-vortex (AV-DWs) domain walls associated with Walker breakdown.³¹ Depending on the strength field, the DW propagation shows three different regimes that affects its velocity.^{28,32–34} At low magnetic fields, typically up to 10 Oe, below the Walker breakdown threshold, the steady motion is governed by viscous DW propagation in which the DW mobility is positive.

The velocity is found to increase linearly as a function of magnetic field. The route to applications depends on stable structure and fast DW motion propagation. However, above the Walker breakdown field, for a wide field range, the DW velocity is reduced, leading to negative DW mobility. The regime is known as precessional or oscillatory. By applying further magnetic field, the DW accelerates, increasing its velocity but slower than the steady regime. For many applications, this behavior is inefficient. In turn, this variability of the domain wall structure affects the pinning behavior as the micromagnetic DW structure present when a wall interacts with a pinning site determines the pinning or de-pinning behavior that occurs. Thus, both the wall velocity and the wall structure need to be stabilized for reliable device operation.

This work addresses a detailed study of domain wall reversal in planar nanowires that combines the experimental measurements and micromagnetic simulations to investigate the role of periodic edge-modulated nanowires for the control of DW propagation and wall structure. Quasi-static measurements and micromagnetic simulations were performed to develop a phase diagram of the magnetic field as a function of modulation amplitude. Taking advantage of DW behaviour observed as a function of time, transformative, stable, and turbulent regime were well identified. The results show that the DW velocity, wall structure, and compact DW motion in the stable regime are suitable for a digital operation mode which is sizeable to process and storage information.

The DW behaviour was studied in planar (Ni₈₀Fe₂₀) nanowires with small fixed-angle triangular periodic structuring on both edges. Samples were fabricated by electron beam lithography with deposition and lift-off of magnetron sputter deposited 10 nm thickness (Figure S1³⁵). The edge structured nanowires were terminated with a DW nucleation pad at one end and a long taper at the other end to control the DW nucleation and propagation direction. The spacing between triangle features along the nanowires was 100 nm; this was chosen to be below the typical length of the domain wall in such nanowires.^{36,37} The nanowire was 80 μm long. DW mediated

reversal was studied using focused magnetometry Kerr (MOKE) with a laser spot size on sample surface of $5\ \mu\text{m}$,³⁸ and measurements of the magnetization reversal were made at different positions along the length of the nanowires, which demonstrated uniformity of the reversal behaviour (Figure S2³⁵). To reduce the stochastic distribution on reversal fields in the DW propagation process, hysteresis were performed on 5 nanowires. This procedure was useful to minimize any further variations from local roughness or defects that could mask the main effects.

Figs. 1(a) and 1(b) show examples of the reversal process measured by MOKE for nanowires with 30 nm and 75 nm amplitude periodic triangular features. The figure also shows schematic illustrations of the nanowire designs above the hysteresis loops. The square shape and sharp reversal of the hysteresis loops are typical for DW mediated reversal in such nanowires. The single sharp magnetization reversal implies that reversal field does not have any dependence on the initial DW chirality. The reversal field is observed to be dependent on the amplitude, indicating that the triangular features acts to prevent wall motion until larger fields are attained. To explore this behaviour, magnetization reversal was measured for a range of triangular modulation amplitudes, as it is shown in Fig. 1(c). The influence of triangular modulation features on the DW reversal behaviour was also studied by means of micromagnetic simulations, which were performed using the Mumax³ code, to investigate the mechanisms occurring in the experiments³⁹ (see Fig. 1(d)). The typical parameters for NiFe were used to carry out the micro-magnetic simulations. They are exchange constant $A = 13 \times 10^{-12}\ \text{J/m}$, saturation magnetization $M_s = 860 \times 103\ \text{A/m}$, and zero magnetocrystalline anisotropy. The NiFe thickness was 10 nm for all nanowires $5\ \mu\text{m}$ long with triangular modulated edges varying between 0 nm up and 75 nm. The simulations were discretized in cells size of $5 \times 5 \times 10\ \text{m}^3$. The Mumax3 code mimic an infinitely long wire by fixing the end spins to avoid any further dipolar

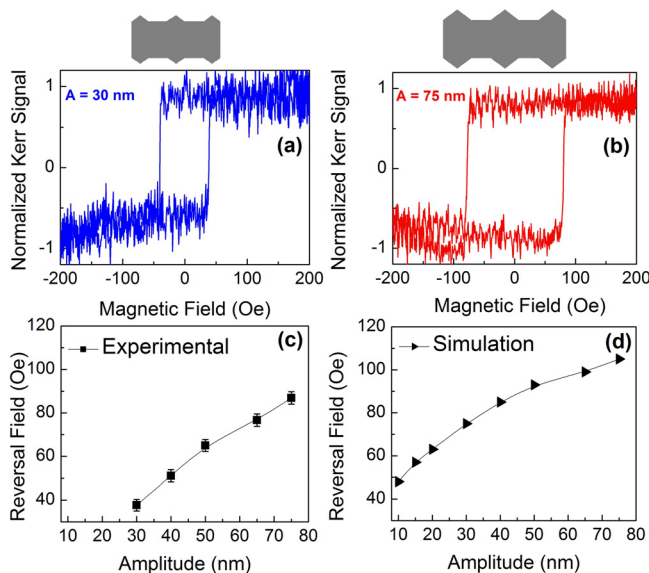


FIG. 1. Examples of hysteresis measured in nanowires with (a) 30 nm and (b) 75 nm triangular amplitude. (c) The measured reversal field as a function of the triangular amplitude and (d) the reversal fields calculated from micromagnetic simulations of comparable nanowires with triangular features as function of the triangular amplitude.

influence. T-DWs were created at $1\ \mu\text{m}$ distant from the nanowire end using high damping 0.5 at zero magnetic field. After DW creation, the magnetic damping was changed to 0.01 to study the DW dynamics motion. The magnetic field thus was applied in the same direction of the main nanowire axis in steps of 1 Oe up to 200 Oe.

In both, the experimental measurements and the micromagnetic simulations, the DW reversal field increases monotonically, but not linearly, with increasing amplitude of the triangular features up to 75 nm. The reversal fields are slightly larger for the simulations. A possible reason for this might be the lack of thermal activation in the micromagnetic simulations that usually increases the coercive field.⁴⁰ For larger amplitude features, the reversal field reaches a peak then falls to an intermediate value in both the measurements and simulations, although the reversal field maximum occurred at a higher modulation amplitude for the simulations. This regime is not considered further here.

The behaviour observed in the DW reversal process suggests that the amplitude periodic triangular features yields a potential barrier to the DW propagation compared to the parallel-sided wires, which makes sense if the triangular features are considered like anti-notches that tend to trap the DW.^{41,42} To overcome this pinning, the magnetic field must be increased, leading to the DW propagation. More importantly, the role of the periodic triangular features for controlling the DW micromagnetic structure and hence the DW stability is also linked with reversal field strength.

A direct comparison of modeling for the DW motion in parallel-sided and edge-modulated nanowires aids understanding the DW reversal mechanisms observed in both geometries. In this case, it is important to know how the strength of the magnetic field affects the magnetic components during DW motion and the DW velocity. Fig. 2(a) shows the time evolution of magnetization components M_x , M_y in the nanowire during DW propagation in a parallel-sided nanowire. It is observed that the M_y component switches between positive and negative values. These oscillations are related to transition from T-DWs-up to T-DWs-down via V-DWs and AV-DWs nucleation, and are identified by arrows in the M_x time dependence. The direction of the arrow indicates the sense of the T-DW chirality. Snapshots of the micromagnetic structures are shown in Figure S3.³⁵ The time evolution of the M_x component also shows that the DW moves back-and-forth along the wire, slowing the average velocity during an average period, $\Delta T^{\text{accel}} = 3\ \text{ns}$. Whilst owing to nucleation of a V-DW or AV-DW, the wall stops with an average period $\Delta T^{\text{retrog}} = 1.5\ \text{ns}$. Indeed, the oscillations and loss of DW velocity represent Walker breakdown and occur above a characteristic Walker breakdown field, indicated by the velocity peak in Fig. 2(d).

Increasing the field beyond the Walker breakdown, the DW velocity falls to a minimum value which, for a range of magnetic field, remains low. With further increase in magnetic field, the DW velocity increases again, but its amplitude is lower compared to the Walker breakdown field. In addition to the low velocity in this oscillatory regime, the DW structure is of course highly variable, and the specific micromagnetic will affect the interaction of the propagating

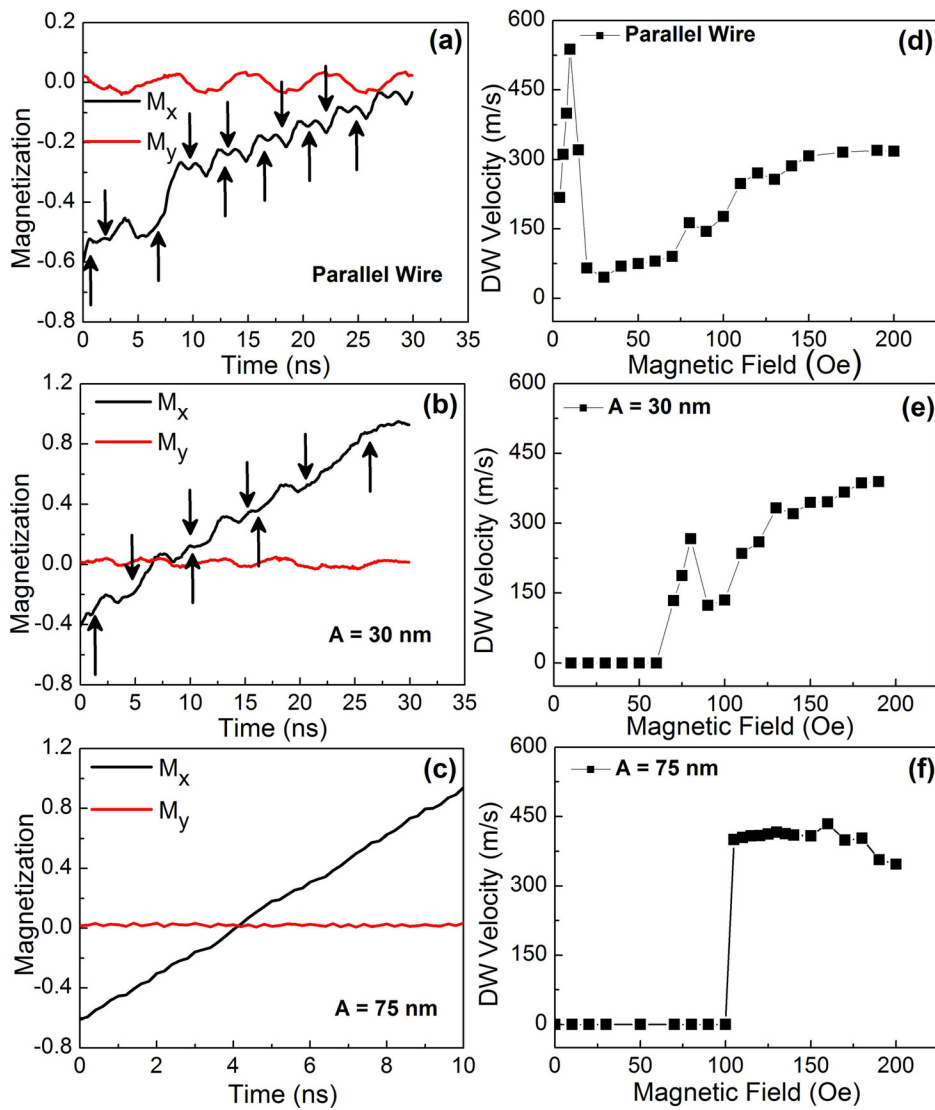


FIG. 2. Magnetic components calculated from micromagnetic simulations in parallel (a), modulated 30 nm (b), and 75 nm nanowires (c). The M_y components alternate between positive and negative values for parallel nanowires and 30 nm amplitude whereas to 75 nm shows roughly positive values. (a) The time evolution for M_x in parallel nanowire oscillates due to retrograde DW motion. (b) A similar behavior is observed to 30 nm amplitude. (c) Unlike to 75 nm, the M_x increases without any oscillations. (d) DW velocity calculated in parallel, and (e) 30 nm amplitude modulated edges, decreases at higher magnetic fields. (f) Increasing the modulated edges amplitude to 75 nm, the DW velocity remains constant at higher magnetic field.

DW with a pinning site, and hence reduce the reliability of controlling the DW pinning.

By including small periodic triangular modulation features of 30 nm amplitude on the nanowire edges, the DW structure oscillations in the magnetization reversal are reduced, as shown in Fig. 2(b). The M_y component remains unchanged for a longer time compared with the parallel wire-sided, reducing the frequency of transitions from T-DW up to T-DW-down. Oscillations were observed for the DW propagation with 30 nm features, as shown by the arrows indicating the retrograde motion in the M_x time evolution. The time scale in this case was also an average $\Delta T^{\text{retrog}} = 1.5$ ns. This affects the DW velocity, as seen in Fig. 2(e). Also, with 30 nm triangle features, the DW was pinned below a field of 70 Oe. Above the pinning field, the DW moves through the nanowire at a velocity that initially increases linearly up to a peak, before dropping down with a similar trend to that observed in the parallel-sided nanowire. The velocity then increases with a further increase in the magnetic field.

By further increasing the amplitude of the structural modulation, the oscillatory DW can be prevented, and this gives control of DW velocity behavior (see Figs. 2(c) and 2(f)) and gives stability to the structure of the propagating DW, which is required for reliable pinning. M_x increases

linearly as a function of time, and both M_y and M_x are largely invariant. Compared with M_x evolution in Figs. 3(a) and 3(b), no oscillation was observed. The depinning field is, however, larger. Below the depinning field, the velocity is zero, but when the magnetic field is sufficient to allow the DW depinning, the velocity is high and remains constant even over a wide magnetic field range. This field-independent DW velocity behavior is observed over a 50 Oe wide range of magnetic field, which is desirable for functional performance in many applications where uniformity of the magnetization reversal is required. Furthermore, the DW micromagnetic structure is also stable across this field range which again is beneficial for reliable application in the DW-based devices. It is important to take account that the NiFe thickness plays a dominant role on the DW velocity (Figure S4³⁵). Increasing the NiFe thickness, the DW velocity decreases and affects its structure and stability. Thus, for thicker NiFe, in the range of magnetic field and amplitude, the instability would take place.

The DW behaviour that emerges from the micromagnetic analysis of nanowires with this structural feature gives insight into the DW reversal regimes that occur. This analysis is summarised in a phase diagram that shows the reversal regimes in terms of the reversal field and the amplitude of

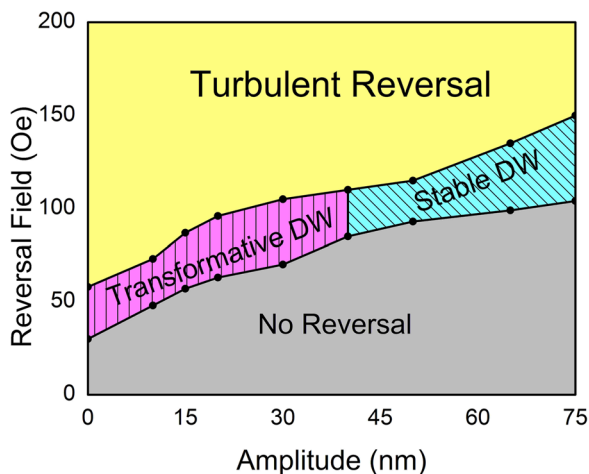


FIG. 3. DW diagram phase propagation regime depending on reversal field and amplitude. At low amplitudes, above reversal field, the transformative and turbulent regimes are observed. An evolution from transformative to stable can be seen between 40 nm and 75 nm amplitudes depending of the magnetic field strength.

the edge features (see Fig. 3). Note first, the transition between pinning and reversal, as indicated by the line between the regions, increases with amplitude and links directly to the reversal fields observed in the experimental work and the micromagnetic simulations shown in Figs. 1(c) and 1(d). The phase diagram shows three reversal regimes. For modulation amplitudes between 0 (parallel) and 40 nm, above the reversal field, the magnetization switching occurs by DW propagation, in which the wall structure undergoes a series of oscillations which affect both the wall velocity and leads to an unstable micromagnetic DW structure. This is the transformative DW regime. For modulation amplitudes above 40 nm, a stable DW reversal regime occurs above the depinning field. In this regime, the wall velocity is largely invariant with the field, and the domain wall structure is highly stable during propagation. In this regime, even far above the reversal field, the DW chirality was conserved. The DW carries its initial chirality along of whole nanowire. At higher fields, for all amplitudes, single DW-mediated reversal is replaced by a turbulent switching regime in which reversal is nucleated in many places along the nanowires.

In summary, the DW motion in nanowires with periodic modulated features edges was studied by experimental and micromagnetic simulations. By means of hysteresis measurements, the reversal field was determined as a function of amplitude as a route to controlling the behaviour on the magnetization reversal in the DW propagation mode. Micromagnetic simulations were carried out to understand the trend observed experimentally and to develop a diagram phase that demarcates the regime of the DW reversal behavior. For small triangular amplitude, below 40 nm, the transformative and turbulent propagation regimes were observed. For larger amplitude features within a specific magnetic field range, a regime of stable, constant velocity DW-mediated was identified. The DW velocity remains constant at higher magnetic fields showing a controlled DW structural and digital operation mode. This result opens an additional route for the reliable control DW propagation and pinning that will be applicable to nanowire DW devices.

We gratefully acknowledge the Brazilian agencies CNPq for providing fellowship to J. Brandão.

- ¹D. A. Allwood, G. Xiong, M. D. Cooke, C. C. Faulkner, D. Atkinson, N. Vernier, and R. P. Cowburn, *Science* **296**, 2006 (2002).
- ²J. H. Franken, H. J. M. Swagten, and B. Koopmans, *Nat. Nanotechnol.* **7**, 499–503 (2012).
- ³S. S. P. Parkin, M. Hayashi, and L. Thomas, *Science* **320**, 190–194 (2008).
- ⁴M. Hayashi, L. Thomas, R. Moriya, C. Rettner, and S. S. P. Parkin, *Science* **320**, 209 (2008).
- ⁵D. A. Allwood, G. Xiong, C. C. Faulkner, D. Atkinson, D. Petit, and R. P. Cowburn, *Science* **309**, 1688 (2005).
- ⁶L. Thomas, M. Hayashi, X. Jiang, R. Moriya, C. Rettner, and S. S. P. Parkin, *Nature* **443**, 197 (2006).
- ⁷L. Thomas, M. Hayashi, X. Jiang, R. Moriya, C. Rettner, and S. Parkin, *Science* **315**, 1553 (2007).
- ⁸M. Hayashi, L. Thomas, C. Rettner, R. Moriya, X. Jiang, and S. S. P. Parkin, *Phys. Rev. Lett* **97**, 207205 (2006).
- ⁹S. Goolaup, M. Ramu, C. Murapaka, and W. S. Lew, *Sci. Rep.* **5**, 9603 (2015).
- ¹⁰C. Murapaka, P. Sethi, S. Goolaup, and W. S. Lew, *Sci. Rep.* **6**, 20130 (2016).
- ¹¹H. Corte-León, A. Beguivin, P. Krzysteczko, H. W. Schumacher, A. Manzin, R. P. Cowburn, V. Antonov, and O. Kazakova, *IEEE Trans. Magn.* **51**, 4001304 (2015).
- ¹²C. Guite, I. S. Kerk, M. C. Sekhar, M. Ramu, S. Goolaup, and W. S. Lew, *Sci. Rep.* **4**, 7459 (2014).
- ¹³H. Corte-León, V. Nabaeci, A. Manzin, J. Fletcher, P. Krzysteczko, H. W. Schumacher, and O. Kazakova, *Sci. Rep.* **4**, 6045 (2014).
- ¹⁴J. H. Franken, M. Herps, H. J. M. Swagten, and B. Koopmans, *Sci. Rep.* **4**, 5248 (2014).
- ¹⁵S. Emori, U. Bauer, S. M. Ahn, E. Martinez, and G. S. D. Beach, *Nat. Mater.* **12**, 611 (2013).
- ¹⁶S. Pizzini, J. Vogel, S. Rohart, L. D. Buda-Prejbeanu, E. Juvé, O. Boulle, I. M. Miron, C. K. Safeer, S. Auffret, G. Gaudin, and A. Thiaville, *Phys. Rev. Lett.* **113**, 047203 (2014).
- ¹⁷R. Tomasello, E. Martinez, R. Zivieri, L. Torres, M. Carpentieri, and G. Finocchio, *Sci. Rep.* **4**, 6784 (2014).
- ¹⁸W. Kang, Y. Huang, C. Zheng, W. Lv, N. Lei, Y. Zhang, X. Zhang, Y. Zhou, and W. Zhao, *Sci. Rep.* **6**, 23164 (2016).
- ¹⁹M. Diegel, R. Mattheis, and E. Halder, *IEEE Trans. Magn.* **40**, 2655 (2004).
- ²⁰J. S. Kim, M. A. Mawass, A. Bisig, B. Krüger, R. M. Reeve, T. Schulz, F. Büttner, J. Yoon, C. Y. You, M. Weigand, H. Stoll, G. Schütz, H. J. M. Swagten, B. Koopmans, S. Eisebitt, and M. Klau, *Nat. Commun.* **5**, 3429 (2014).
- ²¹H. Sohn, M. E. Nowakowski, C. Y. Liang, J. L. Hockel, K. Wetzlar, S. Keller, B. M. McLellan, M. A. Marcus, A. Doran, A. Young, M. Klau, G. P. Carman, J. Bokor, and R. N. Candler, *ACS Nano* **9**(5), 4814 (2015).
- ²²H. Corte-León, B. Gribkov, P. Krzysteczko, F. Marchi, J. F. Motte, H. W. Schumacher, V. Antonov, and O. Kazakova, *J. Magn. Magn. Mater.* **400**, 225–229 (2015).
- ²³B. Issa, I. M. Obaidat, B. A. Albiss, and Y. Haik, *Int. J. Mol. Sci.* **14**, 21266 (2013).
- ²⁴S. F. Zhang, W. L. Gan, J. Kwon, F. L. Luo, G. J. Lim, J. B. Wang, and W. S. Lew, *Sci. Rep.* **6**, 24804 (2016).
- ²⁵D. M. Burn and D. Atkinson, *Appl. Phys. Lett.* **102**, 242414 (2013).
- ²⁶J. Brandão, R. L. Novak, P. R. Soledade, A. Mello, F. Garcia, and L. C. Sampaio, *J. Appl. Phys.* **116**, 193902 (2014).
- ²⁷V. Estevez and L. Laurson, *Phys. Rev. B* **91**, 054407 (2015).
- ²⁸T. J. Hayward, *Sci. Rep.* **5**, 13279 (2015).
- ²⁹V. D. Nguyen, O. Fruchart, S. Pizzini, J. Vogel, J. C. Toussaint, and N. Rougemaille, *Sci. Rep.* **5**, 12417 (2015).
- ³⁰S. Krishnia, I. Purnama, and W. S. Lew, *Appl. Phys. Lett.* **105**, 042404 (2014).
- ³¹A. Thiaville and Y. Nakatani, *Topics in Applied Physics* (Springer, New York, 2006), Vol. 101, p.161.
- ³²D. Atkinson, D. A. Allwood, G. Xiong, M. D. Cooke, C. C. Faulkner, and R. P. Cowburn, *Nat. Mater.* **2**, 85 (2003).
- ³³G. S. D. Beach, C. Nistor, C. Knutson, M. Tsoi, and J. L. Erskine, *Nat. Mater.* **4**, 741–744 (2005).
- ³⁴A. Mougín, M. Cormier, J. P. Adam, P. J. Metaxas, and J. Ferr, *Europhys. Lett.* **78**, 57007 (2007).

- ³⁵See supplementary material <http://dx.doi.org/10.1063/1.4960201> at for domain wall micro-magnetic analyses and additional experimental data.
- ³⁶Y. Nakatani, A. Thiaville, and J. Miltat, *J. Magn. Magn. Mater.* **290**, 750–753 (2005).
- ³⁷L. K. Bogart, D. Atkinson, K. O'Shea, D. McGrouther, and S. McVitie, *Phys. Rev. B* **79**, 054414 (2009).
- ³⁸D. A. Allwood, G. Xiong, M. D. Cooke, and R. P. Cowburn, *J. Phys. D: Appl. Phys.* **36**, 2175 (2003).
- ³⁹A. Vansteenkiste and B. Van de Wiele, *J. Magn. Mater.* **323**, 2585 (2011), see <http://mumax.github.io/3> for more information on Mumax performance.
- ⁴⁰J. G. Deak, *J. Appl. Phys.* **93**, 6814 (2003).
- ⁴¹L. J. Chang, Y. D. Yao, P. Lin, and S. F. Lee, *IEEE Trans. Magn.* **47**, 2519–2521 (2011).
- ⁴²S. J. Noh, Y. Miyamoto, M. Okuda, N. Hayashi, and Y. Keun Kim, *J. Appl. Phys.* **111**, 07D123 (2012).